AIMS Materials Science, 7(2): 130–143.
DOI: 10.3934/matersci.2020.2.130
Received: 20 December 2019
Accepted: 20 March 2020
Published: 25 March 2020

http://www.aimspress.com/journal/Materials

Research article

Electrospinning process control for fiber-structured poly(Bisphenol A-co-Epichlorohydrin) membrane

Wisawat Keaswejjareansuk[1], Xiang Wang[2], Richard D. Sisson[1] and Jianyu Liang[1,*]

[1] Department of Mechanical Engineering, Worcester Polytechnic Institute, 100 Institute Road, Worcester, MA 01609, USA
[2] School of Materials Science and Technology, Wuhan University of Technology, 122 Luoshi Road, Hubei Province 430070, P.R. China

* **Correspondence:** Email: jianyul@wpi.edu; Tel: +15088316649; Fax: +15088315633.

Abstract: Porous and fiber structures are utilized to create lightweight materials for many applications. Poly(bisphenol A-co-epichlorohydrin) PBE or phenoxy resin is a widely used thermoplastic resin in thermoplastic, blends, and polymer matrices. In this article, PBE was selected as a model thermoplastic to fabricate a porous membrane with suitable structure and properties through an electrospinning process. The morphology of the electrospun membrane was effectively controlled by adjusting solution concentration and solvent composition and regulating acceleration potential, while keeping the solution feed rate and tip-to-collector distance at specific values. It was observed that the elastic modulus and tensile strength of the obtained porous PBE membranes were dependent on structure and form. With consistent fiber morphology, the research process obtained a relatively high elastic modulus, tensile strength, and density at 9.125 ± 2.573 GPa, 1.260 ± 0.195 MPa, and 0.420 ± 0.056 g/cm^3, respectively. Thermal analysis showed insignificant differences in the thermal stability between the electrospun samples and raw materials.

Keywords: electrospinning; fiber; poly(bisphenol A-co-epichlorohydrin); porous membrane; thermoplastic; structure property; mechanical property

1. Introduction

Thermoplastic is extensively used in many applications such as consumer products, biomedical materials, chemical sensors, filtration and separation, data storage and transmission, energy materials,

and in the manufacturing process [1–4]. In addition to the ease of processing, mechanical performance is an important factor for thermoplastic utilization. Adding fiber materials and forming fiber composite thermoplastics to improve mechanical properties is a widely applied and well-documented practice [5–10]. Interestingly, recently it was shown that fiber-structured thermoplastics demonstrated significant improvement in mechanical properties compared with the same material having a non-fiber structure. For example, studies of Alexander and Wanasekara showed that the polypropylene PP fibers had tensile strength as high as 200 MPa [5,6]. Ye demonstrated that the polyethylene PE fibers had tensile strength in a range of 26 MPa–3.3 GPa, depending upon the production process, while non-fiber-structured, injection-molded, high-density polyethylene HDPE had a tensile strength of less than 50 MPa [6].

Electrospinning (ES) is an efficient and versatile process to fabricate highly porous membranes [11]. It is a straightforward technique to create continuous fibers with diameters ranging from nano- to micrometers. In this process, a high electric potential is applied to a spinneret (needle), which is connected to a syringe that holds a polymer solution. The polymer solution is fed by a syringe pump to be spun in the applied electric field. During the spinning process, the charged polymer solution is elongated to fiber-like jets and then collected on a grounded collector. The ES process has been studied for many applications, such as biomaterials, batteries, capacitors, catalysts, and filtration systems [12–16]. Several thermoplastic materials have been deployed to create various ES membranes. A summary of the ES-thermoplastics, solvent system, and applications are shown in Table 1.

Table 1. A summary of electrospun thermoplastic materials and their applications.

Material	Solvent	Fiber diameter (μm)	Applications
Polyvinylidene difluoride PVdF [17,18]	*N,N*–dimethylacetamide DMAc	0.40–0.51	Battery separator; polymer electrolyte
	DMAc/acetone	0.38	Microfiltration membrane
	N,N–dimethylformamide DMF	0.50	Membrane distillation
Polyacrylonitrile PAN [19]	DMF	0.75	Ultrafiltration membrane
Polyethylene oxide PEO [20]	Water	0.27–0.40	Biomedical applications; solid-polymer electrolyte
Polyvinyl alcohol PVA [21]	Water	0.08–0.24	Biomedical applications; filtration membrane
Polypropylene PP [22]	Decalin	0.80	Battery separator; filtration membrane; protective clothing
PAN/PVA [18]	DMF (PAN); water (PVA)	0.15	Ultrafiltration membrane
Polyamide-6 PA-6 [23]	Formic acid	0.17	Air filtration membrane
Polyimide PI [23]	DMF	0.30	High temperature resistance, air filtration membrane

Poly(bisphenol-A-co-epichlorohydrin) PBE, or phenoxy resin, is a copolymer of bisphenol-A with epichlorohydrin and is a widely-used thermoplastic resin. It is ductile, tough, and miscible with various polymers, due to the presence of a pendant hydroxyl group (proton donor with appropriate functional groups) [24–27]. It has been shown to increase the glass-transition temperature of functional polymer blends, such as in thermal-responsive, shape-memory applications [25–29]. It has been used to increase the tensile strength, elongation, elastic modulus, and flexural strength in

polymer blends [30–33]. The PBE composites, and the blends with carbon nanotubes, have shown an improvement in storage modulus [34,35]. PBE is also used for increasing the fracture toughness as a polymer matrix and a modifier for cryogenic applications [36,37]. The PBE matrix exhibits significant dispersion of organic modified red mud and enhanced overall thermal stability of organic-inorganic composites [38]. In addition to being a vital component in polymer blends and composites, the PBE-based materials were used as coating agents and binders to improve interfacial adhesion of carbon–fiber-reinforced thermoplastic composites and have gained interest as high-performance composites for aerospace applications [39–41].

In this study, PBE was selected as a model thermoplastic, and a PBE-porous membrane was created using the ES process. Various microstructures with different densities, elastic modulus, and tensile strength were obtained, by adjusting the concentration of the polymer solution, the solvent system, and acceleration potential. Membrane morphology and mechanical and thermal properties were studied, using scanning electron microscopy (SEM), tensile testing, and thermogravimetric analysis (TGA), respectively. This study shows that a consistent fiber structure resulted in higher Young's Modulus and tensile strength, compared with those of other morphologies. This study also identifies the process parameter ranges that reliably resulted in consistent fiber morphology in PBE material.

2. Materials and methods

2.1. Materials

Poly(bisphenol A-co-epichlorohydrin) (PBE, Mw = 40000 g/mol, T_g ~ 108 ^oC [42]), acetone (laboratory standard) and *N,N*–dimethylformamide (DMF, anhydrous 99.8%) were purchased from Sigma–Aldrich and used as received.

2.2. Electrospinning experiments

The study was conducted in two stages. In stage one, the goal was to identify a suitable solvent composition. Variable acetone:DMF (%, v/v) ratios were studied, in order to identify a desirable solvent ratio for creating consistent fiber structures. Acetone:DMF (%, v/v) ratios were varied from 0:100 to 80:20, with an incremental step of a 10% increase in acetone and a 10% decrease in DMF for each data point. DMF was gradually added to the acetone and stirred, until forming a homogeneous solution. Then 0.200 g/mL of PBE was dissolved in these acetone:DMF-solvent solutions for the ES experiments. The obtained polymer solution was loaded into a 10 mL syringe, equipped with a stainless-steel gauge 18 blunt-tip needle (0.838 mm, inner diameter). The polymer solution was fed at a feeding rate of 0.3 mL/h. An acceleration potential of 25 kV was applied at the needle-tip against the collector. A stationary aluminum foil collector was set up at 15 cm (tip-to-collector distance) from the needle tip. Electrospinning experiments were conducted at 23–25 ºC and 50–55% relative humidity.

In stage two, after a suitable acetone:DMF ratio was identified, different PBE concentrations were investigated, including 0.125, 0.150, 0.175, 0.200, 0.225, and 0.250 g/mL, at two different acceleration potentials, 20 kV and 25 kV.

2.3 Characterizations

Surface micrographs were obtained by a field emission scanning electron microscope (FE-SEM, JEOL 7000F), operated at 2 kV. Average density of the membrane spun with each solution concentration was calculated by the weight and volume of three ES samples with an identical diameter of 7/32 inch (0.56 cm). Mechanical properties were measured by a universal testing machine (UTM, Instron 5567A) with a cross-head speed of 2 mm/min. The samples that were used to perform mechanical property measurements were prepared following the previously reported electrospinning studies [43–46]. Each ES membrane was cut into a strip of 0.25 inches (0.63 cm) width, 1 inch (2.54 cm) length, with 0.5 inches (1.27 cm) gauge-length and approximate 65 μm thickness. Each ES-sample was obtained after 40 min. of electrospinning. After drying, the thickness of the deposition was ≥65 μm in the thickest portion. A micrometer was used to measure the thickness at different locations in each sample. The portion that had a thickness of approximately 65 μm was chosen and cut into strips for testing. At least three ES samples were measured for each data point. The samples were also analyzed by thermogravimetric analysis (TGA, TA Instrument Q50) in air, in a temperature range of 35–700 ºC, at a heating rate of 10 ºC/min.

3. Results and discussion

3.1. Solvent composition

The use of the acetone and DMF solvent system in this study was informed by the established understanding of the vapor pressure effect. The boiling point and vapor pressures are 56 ºC for acetone vs. 153 ºC for DMF, and 30.79 kPa for acetone vs. 0.49 kPa for DMF, at 25 ºC, respectively [47,48]. Acetone has a relatively high vapor pressure, at 25 ºC. Hence, the acetone evaporated quickly, which was expected to assist in obtaining thin fibers. The DMF, on the other hand, evaporated slowly, which was anticipated to provide flexibility and allow the spun jets to elongate [49–51]. The rheology of the acetone and DMF binary mixture was thoroughly studied [52,53]. Previous research has investigated the effects of vapor pressure, boiling point, and viscosity of the various binary solvents on morphology [49,51,54–57]. As the solution jets were spun in the electric field, the dielectric constant was suspected to be a factor in producing a membrane with the desired morphology. Hence, dielectric constants of the acetone and DMF solvents were provided in this report.

Different acetone:DMF (%, v/v) ratios were studied to identify a suitable solvent ratio for consistent fiber structures. It was found that a minimum of 20% DMF was needed to fully dissolve 0.200 g/mL of PBE and form a homogeneous solution. Vapor pressure of the mixed solvent at each acetone:DMF ratio was the summation of the partial vapor pressure of acetone and DMF, and calculated by Eq 1 [58]. The dielectric constant of the solvent changes as a function of the composition. O. Kolling experimentally determined and calculated the dielectric constants of the acetone:DMF system at 25 ºC by Eq 2, where $X_{Acetone}$ is the mole fraction of acetone [59]:

$$p_{vapor,total} = X_{Acetone} \times p_{vapor,acetone} + X_{DMF} \times p_{vapor,DMF} \quad (1)$$

$$\epsilon = 36.69 - 15.99X_{Acetone} \quad (2)$$

Table 2. Dielectric constant of the mixed solvents at different ratios of acetone:DMF.

Acetone:DMF	Moles of solvent (mol)		Mole fraction	Vapor pressure	Dielectric constant	Membrane structure
% (v/v)	Acetone	DMF	of acetone	(kPa)		
80:20	0.103	0.031	0.769	23.779	24.400	Fiber with large diameter distribution
70:30	0.088	0.045	0.660	20.476	26.143	
60:40	0.073	0.059	0.555	17.298	27.820	Fiber with small diameter distribution
50:50	0.060	0.072	0.454	14.237	29.435	Fiber-bead
40:60	0.047	0.084	0.356	11.288	30.992	
30:70	0.034	0.096	0.263	8.444	32.493	Nonporous membrane; process turned to electrospray
20:80	0.022	0.108	0.172	5.699	33.941	
10:90	0.011	0.119	0.084	3.050	35.339	
0:100	0.000	0.129	0.000	0.490	36.690	

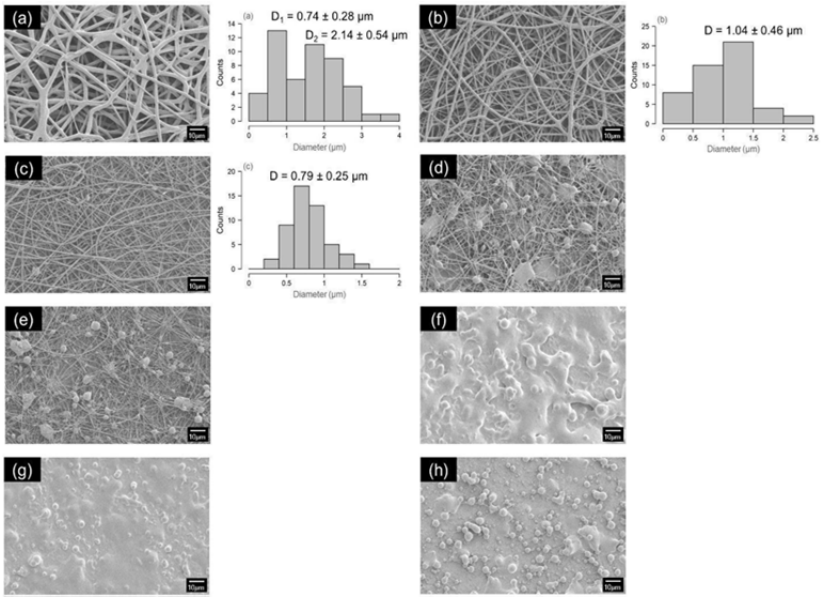

Figure 1. Effect of solvent composition of acetone:DMF (%, v/v) to morphology of the ES-PBE membrane: (a) 80:20; (b) 70:30; (c) 60:40; (d) 50:50; (e) 40:60; (f) 30:70; (g) 20:80; and (h) 10:90 (700× magnification, scale bar corresponds to 10 µm).

Using Eq 2, the dielectric constants of the various solvents tested in this study were calculated and are summarized in Table 2. It was observed that a high dielectric constant resulted in a nonporous membrane. Figure 1 shows the typical morphology of ES-PBE membranes with different solvent ratios. Porous structures of the ES-PBE membrane were obtained, with amounts of DMF up to 60% (Figure 1a–c). Fiber structures were obtained up to a dielectric constant (ϵ of approximately 28 (Table 2). Although a homogeneous solution can be obtained with pure DMF, acetone is required to control the morphology, because acetone evaporates faster than DMF, and the rapid evaporation is needed to reduce the diameter of the spinning jets prior to being collected on the grounded collector. When the amount of acetone was 40–50% (Figure 1d,e), a mixed fiber-bead structure was obtained. When the amount of acetone was less than 40% (Figure 1f–h), there were no fibers observed, and the

membrane became nonporous. A consistently fine fiber structure (Figure 1c) was reliably obtained with an acetone:DMF ratio of 60:40 (%, v/v). Thus, this solvent ratio was selected to be used in future experiments, in order to rule out any variation in solvent composition.

3.2. PBE concentration and acceleration potential

The solvent ratio of 60:40 (%, v/v) acetone:DMF was used in experiments with different concentrations and acceleration potentials. Concentrations ranging from 0.125 to 0.250 g/mL were tested under two acceleration potentials, 20 kV and 25 kV. At low concentrations, ranging from 0.125 to 0.175 g/mL (Figure 2a–c and 2a'–c'), a mixed fiber-bead structure was observed with beads dominant at both acceleration potentials. When the concentrations were increased, this structure gradually transitioned to a fiber-dominant structure. The fiber structure was obtained at concentrations of 0.200–0.250 g/mL (Figure 2d–f and 2d'–f') at both acceleration potentials. At the concentration of 0.200 g/mL, fine and consistent fiber structure was reliably obtained (Figure 2d,d'). At the higher concentration of 0.250 g/mL (Figure 2f,f'), thicker fibers were obtained. At the concentration of 0.125 g/mL, a powder-like deposition was formed on the collector.

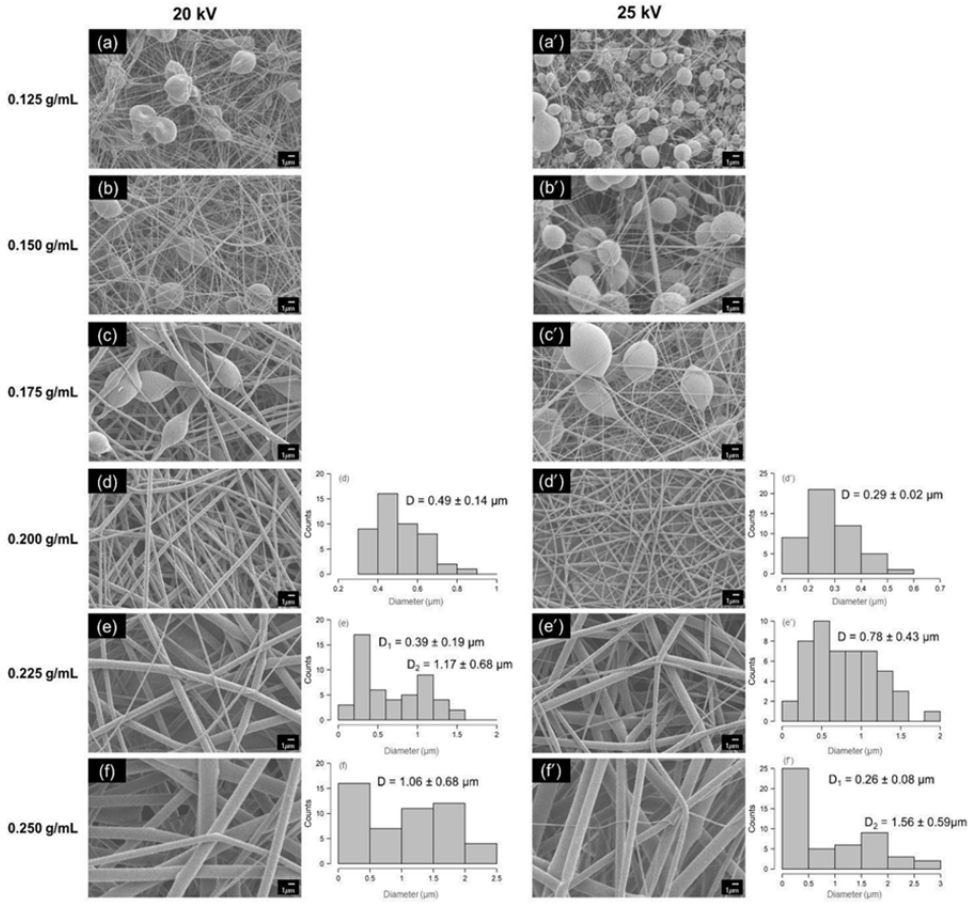

Figure 2. Effects of the concentration and the acceleration potential at 20 kV (a–f) and 25 kV (a'–f') on the morphology: (a) and (a') 0.125 g/mL; (b) and (b') 0.150 g/mL; (c) and (c') 0.175 g/mL; (d) and (d') 0.200 g/mL; (e) and (e') 0.225 g/mL; (f) and (f') 0.250 g/mL (3000× magnification, scale bar corresponds to 1 µm).

It is known that the morphology of the ES membrane may be affected by the acceleration potential. The high acceleration potentials (20 kV and 25 kV) in this study were chosen based on previous studies [21,60,61]. A high-acceleration potential results in a stronger electric field. Hence, the charged solution jets, at high acceleration potential, move faster and produce fibers with a smaller diameter than at the low acceleration potential [61]. The distribution of the fiber diameter (Figure 2d–f and 2d'–f') was measured from 50 different fibers in each SEM figure. The membranes created from the solution concentrations of 0.225 g/mL and 0.250 g/mL had either a wide distribution or showed a bimodal distribution of the fiber diameter. In addition, average fiber diameter expanded with an increase in solution concentration. Similar observations were reported in other studies of electrospun thermoplastics [19,21,61]. The average fiber diameters created from the solution concentration of 0.200 g/mL were 0.49 ± 0.14 μm (spun at 20 kV, Figure 2d) and 0.29 ± 0.02 μm (spun at 25 kV, Figure 2d'). An acceleration potential of 20 kV enables better control over the total deposition thickness, due to a slower deposition rate, as compared with that of 25 kV. In this study, 20 kV was used in subsequent experiments.

3.3. TGA study of ES-PBE membrane

Figure 3 shows the TGA thermogram of the ES-PBE membranes and pellets. The ES-PBE membranes did not show significant weight change until 370 ºC (initial decomposition temperature). Two decomposition steps occurred: the first one at 370–420 ºC and the second one between 480–650 ºC. This observation is similar to Corres' study on thermal decomposition of the PBE powder under ambient atmosphere [27]. Corres et al.'s study shows that the presence of oxygen in an ambient atmosphere affects the degradation behavior and results in two decomposition steps in air, as opposed to a single decomposition step in a nitrogen environment [27].

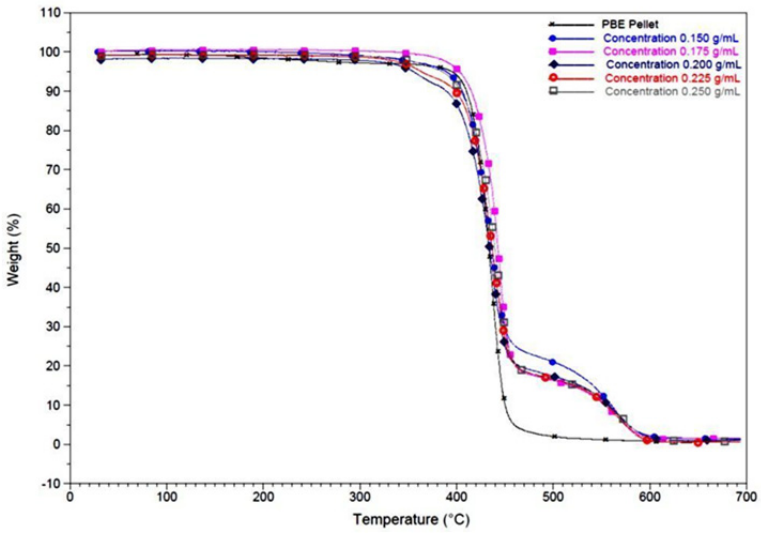

Figure 3. TGA thermogram illustrating thermal decomposition temperatures (~370 ^{o}C) and thermal stability of the ES-PBE membranes.

The ES-PBE membrane was further examined at temperatures slightly higher than the material's glass-transition temperature T_g ~ 108 ºC [42] (Figure 4). Three ES samples, obtained by the same processing conditions (solution concentration = 0.200 g/mL, acceleration potential = 20 kV),

were cut into squares of 2 cm (0.78 inch) by 2 cm. The samples were heated in a box furnace, from room temperature to 110 ºC (slightly higher than the T_g), 115 ^{o}C, and 118 ºC, then held for 1 h. At 110 ºC, a change in the fiber morphology was already noticeable (compared to Figure 2d). At 118 ºC, some fibers were fused together. Even though ES-PBE membranes do not start to decompose until 370 ºC, it is probably necessary to set the service temperature lower than the T_g for applications that demand integrity of the membrane morphology and structure.

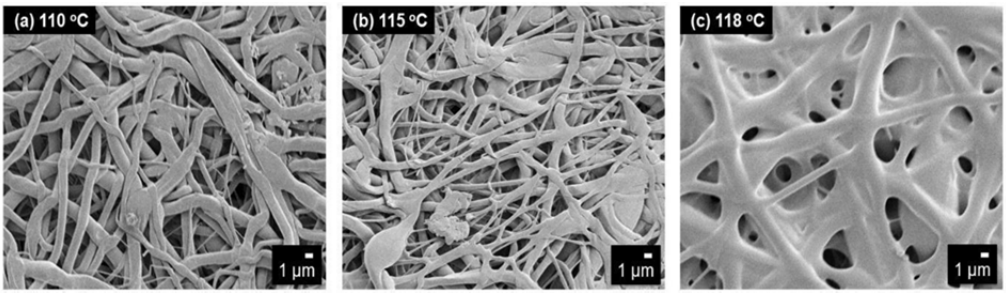

Figure 4. SEM micrographs demonstrate macroscopic morphology deformation of the ES-PBE membrane (solution concentration = 0.200 g/mL, and acceleration potential = 20 kV) at tested temperatures: (a) 110 ºC; (b) 115 ºC; and (c) 118 ºC (3000× magnification, scale bar corresponds to 1 μm).

3.4. Mechanical property

Elastic modulus and tensile strength of the ES-PBE membranes were measured and listed in Table 3. In comparison to the reported nonporous, cast PBE, the electrospun samples had a similar or higher elastic modulus but exhibited lower tensile strength [63]. The relatively large standard deviation of tensile strength and elastic modulus was typical for the ES fibers deposited on the stationary collector, due to the random depositions. This observation agrees with a previous study by Al-Attabi et al. [64]. Differences in the tensile strength between the electrospun membrane and the raw materials have also been seen in previous electrospinning studies on other thermoplastics, for example, PVdF (1.2–7.5 vs 42–43 MPa) and polyvinyl chloride PVC (0.90 vs 56.6 MPa) [65–68]. As presented in Figure 5, membranes with the mixed fiber-bead structure (solution concentrations <0.200 g/mL) had much lower tensile strength than that of the fiber structure (solution concentration ≥0.200 g/mL). Although the tensile strength of the fiber-structured membranes was similar, the membranes with a more consistent fiber structure had a higher elastic modulus (Figure 6). It was observed that the membranes produced from a concentration of 0.200 g/mL had the highest elastic modulus and tensile strength among all the samples tested.

Table 3. Physical and mechanical properties of ES samples, which correspond to different polymer solution concentrations at an acceleration potential of 20 kV.

Concentration of polymer solution (g/mL)	Membrane structure	Average density (g/cm^3)	E (GPa)	TS (MPa)
0.150	Fiber-bead	0.345 ± 0.029	1.129 ± 0.746	0.135 ± 0.065
0.175	Fiber-bead	0.263 ± 0.019	3.322 ± 0.736	0.294 ± 0.022
0.200	Consistent fiber	0.420 ± 0.056	9.125 ± 2.573	1.260 ± 0.195
0.225	Inconsistent fiber	0.368 ± 0.008	2.229 ± 0.994	1.055 ± 0.353
0.250	Inconsistent fiber	0.302 ± 0.005	5.019 ± 2.309	1.271 ± 0.112
PBE pellet	-	1.180 [62]	-	-
Cast PBE (thickness = 120 μm) [63]	Nonporous	-	1.2 [63]	41 [63]

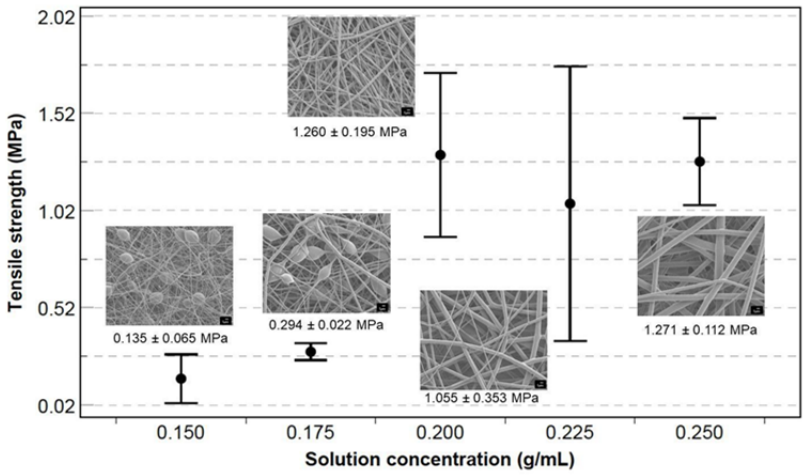

Figure 5. Tensile strength (MPa) correspondence with the polymer solution concentration (g/mL).

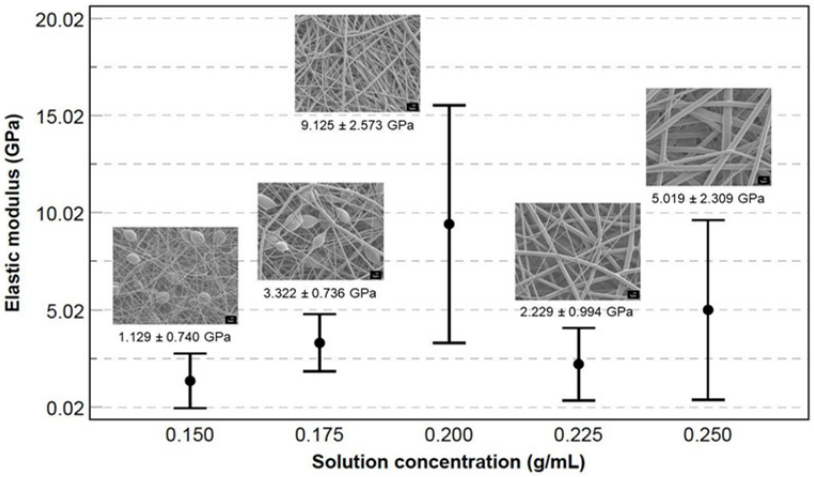

Figure 6. Elastic modulus (GPa) correspondence with the polymer solution concentration (g/mL).

4. Conclusion

In this report, porous PBE membranes were created by an electrospinning process. The thermal stability of the electrospun samples was confirmed to be similar to that of PBE pellets. In this study, the density, tensile strength, and elastic modulus varied, depending on the membrane morphology. Consistent fiber morphology resulted in high tensile strength and elastic modulus. The concentration of polymer solution, solvent composition, and acceleration potential were important factors influencing membrane morphology. Solvent composition determines the dielectric constant, which affects the spinning rate of the solution jets, and, hence, the membrane morphology. In addition, solvent composition is an important parameter for controlling morphology, due to the boiling point and the vapor pressure of each solvent component. PBE is used as an adhesive, coating agent, additive, and matrix to other functional materials. The porous, non-woven membranes of PBEs, with a high thermal stability similar to that of PBE pellets, may be desirable for applications at elevated temperatures that other ES membranes cannot withstand.

Conflict of interests

Authors have declared that no competing interests exist.

References

1. Pang X, Zhuang X, Tang Z, et al. (2010) Polylactic acid (PLA): research, development and industrialization. *Biotechnol J* 5: 1125–1136.
2. Abdelrasoul A, Doan H, Lohi A, et al. (2015) Morphology control of polysulfone membranes in filtration processes: a critical review. *ChemBioEng Rev* 2: 22–43.
3. Gabor H (2000) Polymer films in sensor applications: A review of present uses and future possibilities. *Sens Rev* 20: 98–105.
4. Kang GD, Cao YM (2014) Application and modification of poly(vinylidene fluoride) (PVDF) membranes—A review. *J Memb Sci* 463: 145–165.
5. Wanasekara N, Chalivendra V, Calvert P (2011) Sub-micron scale mechanical properties of polypropylene fibers exposed to ultraviolet and thermal degradation. *Polym Degrad Stab* 96: 432–437.
6. Alexander JV, Neely JW, Grulke EA (2014) Effect of chemical Functionalization on the mechanical properties of polypropylene hollow fiber membranes. *J Polym Sci Pol Phys* 52: 1366–1373.
7. Ye Z, Zhu S, Wang WJ, et al. (2003) Morphological and mechanical properties of nascent polyethylene fibers produced via ethylene extrusion polymerization with a metallocene catalyst supported on MCM-41 particles. *J Polym Sci Pol Phys* 41: 2433–2443.
8. Zhang F, Endo T, Qiu W, et al. (2002) Preparation and mechanical properties of composite of fibrous cellulose and maleated polyethylene. *J Appl Polym Sci* 84: 1971–1980.
9. Shubhra QTH, Alam AKMM, Quaiyyum MA (2013) Mechanical properties of polypropylene composites: A review. *J Thermoplast Compos* 26: 362–391.
10. Bledzki AK, Jaszkiewicz A, Scherzer D (2009) Mechanical properties of PLA composites with man-made cellulose and abaca fibres. *Compos Part A-Appl S* 40: 404–412.

11. Reneker DH, Chun I (1996) Nanometre diameter fibres of polymer, produced by electrospinning. *Nanotechnology* 7: 216–223.
12. Yoshimoto H, Shin YM, Terai H, et al. (2003) A biodegradable nanofiber scaffold by electrospinning and its potential for bone tissue engineering. *Biomaterial*s 24: 2077–2082.
13. Jung JW, Lee CL, Yu S, et al. (2016) Electrospun nanofibers as a platform for advanced secondary batteries: a comprehensive review. *J Mater Chem A* 4: 703–750.
14. Zhang F, Yuan C, Zhu J, et al. (2013) Flexible films derived from electrospun carbon nanofibers incorporated with Co_3O_4 hollow nanoparticles as self-supported electrodes for electrochemical capacitors. *Adv Funct Mater* 23: 3909-3915.
15. Formo E, Lee E, Campbell D, et al. (2008) Functionalization of electrospun TiO_2 nanofibers with Pt nanoparticles and nanowires for catalytic applications. *Nano Lett* 8: 668–672.
16. Gopal R, Kaur S, Ma Z, et al. (2006) Electrospun nanofibrous filtration membrane. *J Memb Sci* 281: 581–586.
17. Choi SS, Lee YS, Joo CW, et al. (2004) Electrospun PVDF nanofiber web as polymer electrolyte or separator. *Electrochimica Acta* 50: 339–343.
18. Vanangamudi A, Yang X, Duke MC, et al. (2019) Nanofibers for membrane applications. In: Barhoum A, Bechelany M, Makhlouf A, *Handbook of Nanofibers*, Springer-Cham, 937–960.
19. Yoon K, Kim K, Wang X, et al. (2006) High flux ultrafiltration membranes based on electrospun nanofibrous PAN scaffolds and chitosan coating. *Polymer* 47: 2434–2441.
20. Deitzel JM, Kleinmeyer JD, Hirvonen JK, et al. (2001) Controlled deposition of electrospun poly(ethylene oxide) fibers. *Polymer* 42: 8163-8170.
21. Zhang C, Yuan X, Wu L, et al. (2005) Study on morphology of electrospun poly(vinyl alcohol) mats. *Eur Polym J* 41: 423–432.
22. Cho D, Zhou H, Cho Y, et al. (2010) Structural properties and superhydrophobicity of electrospun polypropylene fibers from solution and melt. *Polymer* 51: 6005–6012.
23. Al-Attabi R, Morsi YS, Schütz JA, et al. (2018) Electrospun membranes for airborne contaminants capture. In: Barhoum A, Bechelany M, Makhlouf A, *Handbook of Nanofibers*, Springer-Cham, 1–18.
24. Iriarte MA, Iruin JJ, Eguiazábal JI (1989) Thermal decomposition of miscible phenoxy/poly(ethylene oxide) blends. *J Mater Sci* 24: 1021–1024.
25. Zhang R, Luo X, Ma D (1995) Miscibility of polyhydroxy ether of bisphenol-A with ethylene terephthalate-caprolactone copolyesters. *Eur Polym J* 31: 1011–1014.
26. Kim BK, Choi CH (1996) Melt blends of poly(methyl methacrylate) with a phenoxy. *Polymer* 37: 807–812.
27. Corres MA, Zubitur M, Cortazar M, et al. (2011) Thermal and thermo-oxidative degradation of poly(hydroxy ether of bisphenol-A) studied by TGA/FTIR and TGA/MS. *J Anal Appl Pyrol* 92: 407–416.
28. Guo Q (1995) Effect of curing agent on the phase behaviour of epoxy resin/phenoxy blends. *Polymer* 36: 4753–4760.
29. Jeong HM, Ahn BK, Kim BK (2001) Miscibility and shape memory effect of thermoplastic polyurethane blends with phenoxy resin. *Eur Polym J* 37: 2245–2252.
30. Yilmaz T, Özarslan Ö, Yildiz E, et al. (1998) Effects of nonreactive resins on the properties of a UV-curable methacrylated urethane resin. *J Appl Polym Sci* 69: 1837–1845.

31. Qipeng G, Jinyu H, Binyao L, et al. (1991) Blends of phenolphthalein poly(ether ketone) with phenoxy and epoxy resin. *Polymer* 32: 58–65.
32. Choi GD, Kim SH, Jo WH, et al. (1995) The morphology and mechanical properties of phenoxy/liquid crystalline polymer blends and the effect of transesterification. *J Appl Polym Sci* 55: 561–569.
33. Wu H, Ma CM, Lin J (1997) Processability and properties of phenoxy resin toughened phenolic resin composites. *J Appl Polym Sci* 63: 911–917.
34. Yang BX, Shi JH, Pramoda KP, et al. (2007) Enhancement of stiffness, strength, ductility and toughness of poly(ethylene oxide) using phenoxy-grafted multiwalled carbon nanotubes. *Nanotechnology* 18: 125606.
35. Goh HW, Goh SH, Xu GQ, et al. (2003) Dynamic mechanical behavior of in situ functionalized multi-walled carbon nanotube/phenoxy resin composite. *Chem Phys Lett* 373: 277–83.
36. Ueki T, Nojima K, Asano K, et al. (1998) Toughening of epoxy resin systems for cryogenic use. *Adv Cryog Eng Mater* 44: 277–283.
37. Ueki T, Nishijima S, Izumi Y (2005) Designing of epoxy resin systems for cryogenic use. *Cryogenics* 45: 141–148.
38. Bhat AH, Abdul Khalil HPS, Bhat IUH, et al. (2011) Development and characterization of novel modified red mud nanocomposites based on poly(hydroxy ether) of bisphenol A. *J Appl Polym Sci* 119: 515–522.
39. Yi JW, Lee W, Seong DG, et al. (2016) Effect of phenoxy-based coating resin for reinforcing pitch carbon fibers on the interlaminar shear strength of PA6 composites. *Compos Part A-Appl S* 87: 212–219.
40. Beier U, Sandler JKW, Altstadt V, et al. (2009) Mechanical performance of carbon fibre-reinforced composites based on stitched and bindered preforms. *Compos Part A-Appl S* 40: 1756–1763.
41. Beier U, Wolff-Fabris F, Fischer F, et al. (2008) Mechanical performance of carbon fibre-reinforced composites based on preforms stitched with innovative low-melting temperature and matrix soluble thermoplastic yarns. *Compos Part A-Appl S* 39: 1572–1581.
42. Chemical Retrieval on the Web (CROW), Polymer properties database: epoxy or phenoxy resin, 2018. Available from: https://polymerdatabase.com/polymers/bisphenoladiglycidyletherepoxyresin.html.
43. Lee SG, Han KS, Joo CW, et al. (2004) Electrospun PVDF nanofiber web as polymer electrolyte or separator. *Electrochim Acta* 50: 339–343.
44. Hao J, Lei G, Li Z, et al. (2013) A novel polyethylene terephthalate nonwoven separator based on electrospinning technique for lithium ion battery. *J Memb Sci* 428: 11–16.
45. Zhang J, Liu Z, Kong Q, et al. (2013) Renewable and superior thermal-resistant cellulose-based composite nonwoven as lithium-ion battery separator. *ACS Appl Mater Inter* 5: 128–134.
46. Yanilmaz M, Dirican M, Zhang X (2018) Evaluation of electrospun SiO_2/nylon 6,6 nanofiber membranes as a thermally-stable separator for lithium-ion batteries. *Electrochim Acta* 133: 501–508.
47. U.S. National Library of Medicine, Acetone, 2004. Available from: https://pubchem.ncbi.nlm.nih.gov/compound/180.
48. U.S. National Library of Medicine, *N,N*–Dimethylformamide, 2004. Available from: https://pubchem.ncbi.nlm.nih.gov/compound/6228.

49. Thompson CJ, Chase GG, Yurin AL, et al. (2007) Effects of parameters on nanofiber diameter determined from electrospinning model. *Polymers* 48: 6913–6922.
50. Shawon J, Sung C (2004) Electrospinning of polycarbonate nanofibers with solvent mixtures THF and DMF. *J Mater Sci* 39: 4605–4613.
51. Lin J, Ding B, Yu J, et al. (2010) Direct fabrication of highly nanoporous polystyrene fibers via electrospinning. *ACS Appl Mater Inter* 2: 521–528.
52. Gill DS, Sherma AN (1982) Acetone + *NN*–Dimethylformamide solvent system. Part 2—Conductance studies of some electrolytes in Acetone + *NN*–Dimethylformamide mixtures at 25 ºC. *J Chem Soc Faraday Trans* 78: 465–474.
53. Gill DS, Schneider H (1980) Acetone–*N,N*–dimethylformamide solvent system. Part 1—properties of Acetone–*N,N*–dimethylformamide binary mixtures. *Indian J Chem* 19A: 313–316.
54. Yoon K, Hsiao BS, Chu B (2009) Formation of functional polyethersulfone electrospun membrane for water purification by mixed solvent and oxidation process. *Polymer* 50: 2893–2899.
55. Qian YF, Su Y, Li XQ, et al. (2010) Electrospinning of polymethyl methacrylate nanofibers in different solvents. *Irian Polym J* 19: 123–129.
56. Katsogiannis KAG, Vladisavljevic GT, Georgiadou S (2015) Porous electrospun polycaprolactone (PCL) fibres by phase separation. *Eur Polym J* 69: 284–295.
57. Casasola R, Thomas NL, Trybala A, et al. (2014) Electrospun poly lactic acid (PLA) fibres: effect of different solvent systems on fibre morphology and diameter. *Polymer* 55: 4728–4737.
58. Kugel RW (1998) Raoult's law: binary liquid-vapor phase diagrams, a simple physical chemistry experiment. *J Chem Educ* 75: 1125–1129.
59. Kolling OW (1993) Dielectric characterization of cosolvents containing *N,N*–dimethylformamide. *Trans Kansas Acad Sci* 97: 88.
60. Ligneris E, Dumee LF, Al-Attabi R, et al. (2019) Mixed matrix poly(vinyl alcohol)-copper nanofibrous anti-microbial air-microfilters. *Membranes* 9: 87–100.
61. Jacobs V, Anandjiwala RD, Maaza M (2010) The influence of electrospinning parameters on the structural morphology and diameter of electrospun nanofibers. *J Appl Polym Sci* 115: 3130–3136.
62. Sigma-Aldrich, Poly(bisphenol A-co-epichlorohydrin), 2019. Available at: https://www.sigmaaldrich.com/catalog/product/aldrich/181196.
63. Sainsbury T, Gnaniah S, Spencer SJ, et al. (2017) Extreme mechanical reinforcement in graphene oxide based thin-film nanocomposites via covalently tailored nanofiller matrix compatibilization. *Carbon* 114: 367–376.
64. Al-Attabi R, Dumee LF, Schutz JA, et al. (2018) Pore engineering towards highly efficient electrospun nanofibers membranes for ae rosol particle removal. *Sci Total Environ* 625: 706–715.
65. Mark JE (2009). Polymer Data Handbook, 2 Eds., New York: Oxford University Press, 190: 1170.
66. Kim YJ, Ahn CH, Lee MB, et al. (2011) Characteristics of electrospun PVDF/SiO_2 composite nanofiber membranes as polymer electrolyte. *Mater Chem Phys* 127: 137–142.
67. Yang K, Ma X, Chen F, et al. (2017) Preparation and characterization of gel polymer electrolyte based on electrospun polyhedral oligomeric silsesquioxane-poly(methyl methacrylate)8/polyvinylidene fluoride hybrid nanofiber membranes for lithium-ion batteries. *J Solid State Electrochem* 22: 581–590.

68. Lee KH, Kim HY, Ryu YJ, et al. (2003) Mechanical behavior of electrospun fiber mats of poly(vinyl chloride)/polyurethane polyblends. *J Polym Sci Pol Phys* 41: 1256–1262.